Orthotropic Hygroscopic Behavior of Mass Timber: Theory, Computation, and Experimental Validation

Danyang Tong
Northwestern University
Susan-Alexis Brown (susanalexisbrown@u.northwestern.edu)
Northwestern University
Hao Yin
Northwestern University
David Corr
Northwestern University
Eric Landis
University of Maine
Giovanni Di Luzio
Politecnico Milano
Gianluca Cusatis
Northwestern University

Research Article

Keywords: laminated timber, orthotropic, permeability, sorption isotherm

Posted Date: October 17th, 2022

DOI: https://doi.org/10.21203/rs.3.rs-2159913/v1

Orthotropic Hygroscopic Behavior of Mass Timber: Theory, Computation, and Experimental Validation

Danyang Tong[1], Susan-Alexis Brown[1*], Hao Yin[1], David Corr[1], Eric Landis[2], Giovanni Di Luzio[3] and Gianluca Cusatis[1]

[1*]Department of Civil and Environmental Engineering, Northwestern University, 2045 Sheridan Rd, Evanston, 60208, IL, USA.
[2]Department of Civil and Environmental Engineering, University of Maine, 5711 Boardman Hall, Orono, 04469, ME, USA.
[3]Department of Civil Engineering, Politecnico Milano, Piazza Leonardo da Vinci, 32 , Milano, 20133, Italy.

*Corresponding author(s). E-mail(s): susanalexisbrown@u.northwestern.edu;

Abstract

Recent rapid improvements in laminated timber technology has led to the increased use of of wood in both mid- and high-rise construction, generally posed as a more carbon friendly alternative to concrete. However, wood is significantly more sensitive to changes in relative humidity than concrete, which may impact the sustainability and durability of mass timber buildings. Moisture cycling in particular affects not only shrinkage and swelling but also strongly influences wood creep. This sensitivity is of high concern for engineered wood used in mass timber buildings. At the same time, wood, considered as an orthotropic material, exhibits varying diffusivity in all three directions, complicating efforts to characterize its behavior. In this work, an orthotropic hygroscopic model was developed for use in laminated timber. A species database for wood sorption isotherm was created and an existing model was used to fit species-based parameters. Diffusion behavior which considers the sorption isotherm was modeled through numerical simulations, and species-dependent

orthotropic diffusion parameters were identified. A database of permeability in all directions for various species was created. The resulting model is able to predict diffusion behavior in glulam and cross laminated timber (CLT) for multiple species of the lab tests. The model also predicts the moisture ranges for a CLT panel under environmental change with parameters from these sorption isotherm and diffusion databases.

Keywords: laminated timber, orthotropic, permeability, sorption isotherm

Acknowledgements: Financial support from the U.S. National Science Foundation (NSF) under Grant No. CMMI-20 1762757 is gratefully acknowledged.

Competing Interests: The authors declare that they have no confict of interest.

1 Introduction

As demand for high-density construction rises with increasing global population, the embodied carbon of traditional structural materials (steel, concrete) is of increasing environmental concern. For example, cement products produce over 8% of global carbon emissions (Lehne and Preston, 2018). To reduce the environmental impact of concrete and steel, mid-rise building design with carbon sequestering building materials will play a critical role in the environmental impact of buildings. In recent decades, with the development of engineered products such as cross laminated timber (CLT), mass timber now provides high strength and stability, superior fire resistance, long service lives, and effective thermal performance (Sun et al, 2020; Osborne et al, 2012). Mass timber is thus a comparable substitute for mid-rise construction, either wholly replacing concrete, or in hybrid concrete-timber design (Kremer and Symmons, 2015). This is exemplified by the heights reached by modern construction; the tallest pure mass timber building is 81 meters in Brumunddal, Norway (Abrahamsen, 2017), and Ascent, in Milwaukee, USA, is 20 stories of mass timber over five stories of concrete, reaching 87 meters (Fernandez et al, 2020). However, building at that height must take into account creep, shrinkage, and swelling deformations -all influenced by the moisture content- to properly account for long-term sustainability (Žlahtič-Zupanc et al, 2018). Thus a robust prediction of mass transport in laminated timber is necessary for successful mass timber construction.

1.1 Moisture effects in wood

It is well known that wood is a hygroscopic and porous material, and is highly sensitive to humidity. Wood is commonly categorized by hardwood and softwood, which differ somewhat in cell formation and geometry. Longitudinal

cells in softwood, known as tracheids, provides passageways for water conduction through bordered pit chambers (cavities in the lignified cell walls) (Usta, 2005). Hardwood, on the other hand, uses vessel cells to transport moisture. Moisture can also move in the radial or tangential directions, but to a lesser degree. In both cases, water stored in the cell walls is classified as bound water, and moisture gradients causes movement of bound water (Baker, 1956). As mentioned, both swelling and creep in wood depend on moisture content (MC). Orthotropic wood shrinkage behavior is well studied (Silva et al, 2014) and is generally calculated to be linearly related to change in moisture content, approximated as 1% change in cross-section for every 4% change in MC (Ross, 2010).

Wood creep is a more complicated phenomenon compared to shrinkage and swelling, but studies on basic creep are available in the literature (Holzer et al, 1989), and a general prediction model of long term behavior independent of moisture content was developed in Tong et al (2020). However, creep effects associated with transient moisture content, generally known as mechano-sorptive creep, are also relevant. Multiple studies revealed that changing of moisture content leads to significantly larger deformations than under constant moisture content (Hunt, 1999; Ranta-Maunus, 1975; Mukudai and Yata, 1986; Hoffmeyer and Davidson, 1989). Wood creep under mechano-sorptive effect could have a crucial influence on the durability and stability of mass timber buildings when exposed to seasonal changes in relative humidity.

Indeed, multiple studies investigated the climate-induced impacts of moisture movement in laminated wood, and showed that it will have consequential effects on the long-term sustainability of mass timber construction (Autengruber et al, 2020; Pang and Jeong, 2020; Chiniforush et al, 2019). Thus modeling the diffusion of humidity through laminated wood is critical to predicating the long-term behavior in these structures and ensuring sustainable implementation of carbon sequestering construction materials.

1.2 Wood isotherm and diffusion

It is first necessary to understand the interaction and movement of water in wood cells to model moisture transport at larger scales. Freshly cut wood has high a MC comprised of liquid water and water vapor existing in the cell lumens (free water) and in wood cell walls (bound water). Lumber for use in construction is dried before use, from which free water and a portion of the bound water are desorbed. During and post-construction, the moisture content will fluctuate up and down with weather, but cannot pass the fiber saturation point (FSP, 26%-32% MC), up to which no free water exists in wood cells (Skaar, 1988). The water transport processes can thus be separated into two parts: 1) water vapor movement between environment and wood cells, which is known as moisture sorption, and 2) water diffusion inside of wood cells. A moisture sorption isotherm is the curve presenting equilibrium moisture content versus ambient relative humidity at a fixed temperature (Kaymak-Ertekin and Sultanoğlu, 2001). Several empirical and semi-empirical mathematical models

have been proposed to capture the isotherm curve (Brunauer et al, 1938; Dent, 1977; Thémelin, 1998; Oswin, 1946; Merakeb, 2006).

Studies have been performed to developing analytical models to mimic water diffusion inside the wood cells. One theory introduced the coupled processes active in the moisture transport including: 1) diffusion of vapor in vessels; 2) diffusion of bound water in wood cell walls; 3) phase change from one state to the other (Hozjan and Svensson, 2011). There are models which separate the gas and liquid phase of moisture transport, as they are driven by different forces (Abbasion et al, 2015; Autengruber et al, 2020). However, in structural lumber there is no free water participating the water diffusion process (as MC is always below the FSP), and thus no need for consideration of gas and liquid phases distinctly. Therefore, a coupled Fickian model is thus proposed, in which vapor transport in pores and bound water transport in wood tissue are modeled by individual transport equations, both following Fick's law. The transport equations are fully coupled by the process of phase change from vapor to bound water (Hozjan and Svensson, 2011).

As wood is represented as an orthotropic material, water transport in wood cells also behaves orthotropically. The diffusion process is divided into two regimes: 1) parallel diffusion in pores and fibers, where water remains within the same media, such as water diffusion in the longitudinal direction along the wood lumens; 2) series diffusion within pores and fibers, where water moves across wood vessels and cell wall media, such as in the radial and tangential directions (Gezici-Koç et al, 2017). Thus, water diffusion capacity is different along longitudinal, radial, and tangential directions. The variation of diffusion between radial and tangential directions directly results from the internal structure. For example, earlywood cell walls are thinner, and the pores larger, thus permeability is higher than in latewood. Water vapor passes through early wood and latewood alternatively along radial direction, while in tangential direction water follows primarily along either earlywood or latewood cells (Borrega and Kärenlampi, 2011).

1.3 Engineered wood

Engineered wood products used for mass timber buildings include 1) glued laminated timber (glulam), which is composed of layers of dimensional lumber bonded together with structural adhesives, used as one-dimensional elements such as vertical columns, horizontal beams, and arches; 2) two-dimensional elements such as cross laminated timber (CLT), which is composed of longitudinal layers and cross layers with the laminations of the adjoining layers are glued orthogonally, or related products such as nail laminated timber, or dowel laminated timber. These two-dimensional structural members are used for walls, roofs or ceilings. There are studies which have analyzed isotropic moisture transport in one-dimensional laminated wood (Afshari and Malek, 2022). However, the layer arrangement of the orthotropic behaviors of CLT may cause uneven deformation between adjoining layers under changing humidity and temperature (Wood et al, 2018). For example, one layer of CLT may

have a smaller shrinkage coefficient than its adjacent layer. When there is a variation of environmental condition, two elements tend to shrink or swell differently. This will also create stress concentrations in the adhesive and eventual deterioration of the structure (Nakajima et al, 2020).

In this study, an orthotropic hygrothermal model which can be generally applied to laminated wood of various species is developed and verified. A database with fitted parameters in three directions for multiple species was created. The model is successfully applied to predict the water diffusion for both glulam and CLT.

2 Methods

2.1 Moisture Transport Governing Equation

2.1.1 Governing equations

Water which exists in wood lumens and cell walls can be found in both vapor and liquid phases. During wetting or drying, bound water would exchange with free water and water vapor to reach equilibrium with the environment. However, MC in structural application is under the FSP, which means free water and water vapor serve as negligible forms of moisture transport. Instead of exploring the relationship between free water and bound water, it is possible to simplify the process by making an assumption that bound water is interacting directly with the environment, neglecting the transformation from bound water to free water or water vapor. By Fick's Law, the overall process of the moisture transport in orthotropic materials considering the isothermal condition is then given as

$$\mathbf{J} = -\mathbf{D}(T)\boldsymbol{\nabla} h \tag{1}$$

where $\mathbf{J}$, is the flux of water mass per unit time as a function of spatial gradient of relative humidity h. $\mathbf{D}$ (kg/m· s) is a temperature related term, represents different diffusion behaviors in three directions is written as a diagonal matrix:

$$\mathbf{D}(T) = \psi(T)\begin{bmatrix} D_1 & 0 & 0 \\ 0 & D_2 & 0 \\ 0 & 0 & D_3 \end{bmatrix} \tag{2}$$

and

$$\psi(T) = \exp\left(\frac{E_{ad}}{RT_0} - \frac{E_{ad}}{RT}\right) \tag{3}$$

The diagonal matrix is regarded as diffusion at the reference temperature. The coefficient $\psi(T)$ takes into account the effect of temperature on diffusion as earlier proposed by Bažant and Najjar (1972), and later adopted by Di Luzio and Cusatis (2009). T_0 is reference temperature (K), T is the absolute temperature (K), R is the universal gas constant (J·mol^{-1} K^{-1}) and $E_{ad}/R \approx 2700$ K.

Based on the moisture mass balance, the variation in time of the water mass per unit volume of solid will be equal to the divergence of the moisture flux $\mathbf{J}$,

$$-\frac{\partial w}{\partial t} = \boldsymbol{\nabla} \cdot \mathbf{J} \tag{4}$$

where w is the water mass per unit volume (kg/m^3). Substituting Eq. 1 into Eq. 4, one can obtain:

$$\frac{\partial w}{\partial t} = \boldsymbol{\nabla} \cdot (\mathbf{D} \boldsymbol{\nabla} h) \tag{5}$$

However, for wood material, moisture content u is commonly defined as the mass of water per unit mass of oven-dried solid. It is convenient to introduce porosity to convert the governing equation in terms of u.

$$1 - \phi = \frac{V_{dry}}{V_{total}} \tag{6}$$

where V_{dry} is the solid volume of the wood skeleton, while the total volume V_{total} of the sample includes the void volume. Substituting Eq. 6 into Eq. 5 gives the governing equation:

$$\frac{\partial u}{\partial t} = \boldsymbol{\nabla} \cdot (\mathbf{D_u} \boldsymbol{\nabla} h) \tag{7}$$

$\mathbf{D_u}$ is the moisture permeability tensor (m^{2}s^{-1}) and

$$\mathbf{D_u} = \begin{bmatrix} D_{u1} & 0 & 0 \\ 0 & D_{u2} & 0 \\ 0 & 0 & D_{u3} \end{bmatrix} = \frac{\mathbf{D}}{\rho_{dry}(1-\phi)} \tag{8}$$

where ρ_{dry} is the density for oven-dried wood sample. In structural applications, it is more common to measure the environmental relative humidity, h, than the moisture content u. By using the chain rule, Eq. 7 becomes:

$$\frac{\partial u}{\partial h}\frac{\partial h}{\partial t} = \boldsymbol{\nabla} \cdot (\mathbf{D_u} \boldsymbol{\nabla} h) \tag{9}$$

where $u(h)$ is the sorption isotherm.

2.1.2 Sorption isotherm model

The relationship between the relative humidity in the environment and the moisture content inside the wood solid is called sorption isotherm. In this study, the Guggenheim, Anderson, de Boer model (GAB) proposed by Thémelin (1998) was adopted,

$$u = \frac{X_m C K h}{(1 - Kh)(1 + (C-1)Kh} \tag{10}$$

where X_m is the monolayer saturation moisture content (kg$\cdot$ kg^{-1}), C is the Guggenheim constant and K is the constant related to monolayer sorption heat. It has been shown that hardwood is more sensitive to temperature

change than softwood due to the internal structure (Krupińska et al, 2007). The GAB model parameters can also be physically modified for temperature variation as shown in (Vishwakarma et al, 2011), $X_m = X_{m0} \exp\left(\frac{q_m}{RT}\right)$, $K = K_0 \exp\left(\frac{\Delta H_k}{RT}\right)$, $C = C_0 \exp\left(\frac{\Delta H_k}{RT}\right)$, where C_0, K_0, X_{m0} and q_m are empirical constants, and ΔH_k and ΔH_c are functions of the heat of water sorption, J/mol.

2.2 Parameter Identification

2.2.1 Sorption isotherm database

Loss of moisture is termed desorption, and increasing moisture content is termed absorption; there exists a hysteresis between adsorption and desorption. To generalize the model, a database of sorption isotherm curves under room temperature was created, which consists of 37 species including commonly used softwoods and hardwoods in the US, as well as tropical woods. Although adsorption and desorption isotherms are not concurrent, their difference is generally neglected. For this reason, in the following work, sorption isotherm will be used with reference to both adsorption and desorption conditions. Each individual experimental curve was averaged from desorptive and adsorptive behaviors. An example is shown in Fig. 1a.

An unbiased statistical evaluation of weighted least square method was used in this work to quantity the quality of the fit (see Section A). This is to account for the non-uniform distribution of data, as discussed in Bažant and Li (2008). Fitting the averaged desorptive and adsorptive curves, Fig. 1b displays an example of individual curve fitting, and Table 1 presents that individual sorption isotherm parameters for various species. Then all data points were fitted to produce a set of general parameters used for the sorption isotherm in wood: $X_m = 6.35$, $C = 7.818$, $K = 0.785$. The result is shown in Fig. 1c. It is clear that species variation does not result in large differences of the sorption isotherm curves. Furthermore, although there is a hysteresis between adsorption and desorption, the data width is narrow enough to approximation as a single sorption isotherm.

2.2.2 Moisture transport implementation

Once the sorption isotherm parameters were identified, the moisture permeability tensor $\mathbf{D_u}$ is the only unknown material property which needs to be calibrated. The authors used numerical simulations to fit the tensor parameters against a variety of experimental data. The following outlines the finite element implementation used for simulations.

In the 3D setting, the governing equation of mass balance, Eq. 9, can be rewritten as

$$\frac{\partial}{\partial x_1}\left(D_{u1}\frac{\partial h}{\partial x_1}\right) + \frac{\partial}{\partial x_2}\left(D_{u2}\frac{\partial h}{\partial x_2}\right) + \frac{\partial}{\partial x_3}\left(D_{u3}\frac{\partial h}{\partial x_3}\right) + C_1\frac{\partial h}{\partial t} = 0 \quad (11)$$

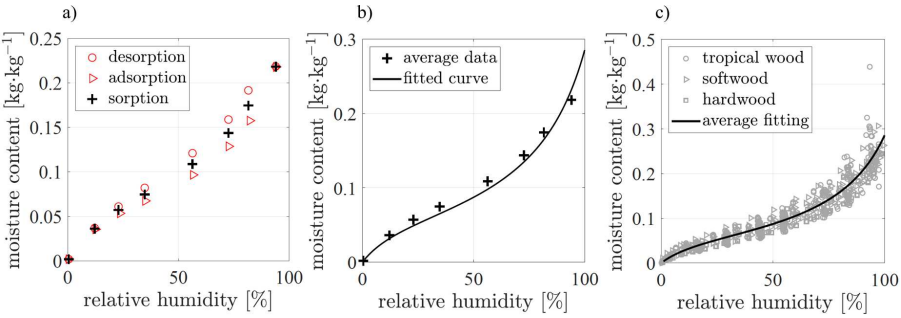

Fig. 1 a) Example averaging adsorption and desorption data; b) fitted example of averaged data; c)isotherm database with fitted curve for all averaged data points. Green is adsoprtion process, yellow is desorption process, and blue is unspecified sorption data points

where x_1, x_2, and x_3 are three orthotropic directions, coefficient $C_1 = -\partial u/\partial h$.

By employing the classical Galerkin finite element method based on the weak formulation associated with the governing equation Eq. 11 (for the detailed derivation, see B), considering only essential boundary conditions and the finite element interpolation of the primary variables, i.e. $h(x_1, x_2, x_3, t) = \sum_i^N h_i(t) N_i(x_1, x_2, x_3)$, where $N_i(x_1, x_2, x_3)$ is the shape function, N is the number of element nodes, one gets

$$\mathbf{M}\dot{\mathbf{h}} + \mathbf{K}\mathbf{h} = \mathbf{0} \tag{12}$$

where the matrices $\mathbf{M}$ and $\mathbf{K}$ are obtained by the assemblage over the entire domain of element level matrices given by

$$\begin{aligned} M_{ij}^e &= \int_{\Omega^e} C_1 N_i N_j \mathrm{d}V \\ K_{ij}^e &= \int_{\Omega^e} \left[-\left(D_{u1} \frac{\partial N_i}{\partial x_1} \frac{\partial N_j}{\partial x_1} + D_{u2} \frac{\partial N_i}{\partial x_2} \frac{\partial N_j}{\partial x_2} + D_{u3} \frac{\partial N_i}{\partial x_3} \frac{\partial N_j}{\partial x_3} \right) \right] \mathrm{d}V \end{aligned} \tag{13}$$

The implementation of the transport model in Abaqus has been performed using Abaqus user defined elements and user subroutines for implicit analyses *UEL*. Generally, in a *UEL*, users should use the incremental form of the governing equations for both linear and nonlinear problems, and provide the Jacobian (a.k.a.the tangent stiffness) matrix *AMATRX* and the right hand side (a.k.a. the residual) vector *RHS* of the incremental governing equations to allow Abaqus to calculate the increments of degrees of freedom of each user defined element.

One can rewrite the governing equation, Eq. 12, as the incremental form using the Newton-Raphson method as: $\mathbf{f}(\mathbf{h}_{n+1}) \approx \mathbf{f}(\mathbf{h}_n) + \frac{\partial \mathbf{f}(\mathbf{h})}{\partial \mathbf{h}}\Big|_n \Delta\mathbf{h} = \mathbf{0}$, by rearranging, one has $\frac{\partial \mathbf{f}(\mathbf{h})}{\partial \mathbf{h}}\Big|_n \Delta\mathbf{h} = -\mathbf{f}(\mathbf{h}_n)$, where $\mathbf{f}(\mathbf{h}) = \mathbf{M}\dot{\mathbf{h}} + \mathbf{K}\mathbf{h}$.

The term $\partial \mathbf{f}(\mathbf{h}) / \partial \mathbf{h}$ is the entry of the Jacobian (tangent stiffness) matrix *AMATRX*, and term $-\mathbf{f}(\mathbf{h}_n)$ is the entry of the right-hand side (residual)

Table 1 Sorption isotherm database and fitted parameters

Class	T (°C)	X_m	C	K	ω	r^2	Source
S	25	5.486	7.940	0.798	0.0383	0.9979	Weichert
S	30	8.010	8.433	0.798	0.0383	0.9979	Fredriksson and Thybring
S	23	8.661	4.036	0.674	0.0200	0.9993	Zhang et al
S	30	5.135	2.592	0.759	0.0182	0.9996	Pittet
S	20	7.022	7.357	0.752	0.0305	0.9977	Hill et al
S	20	6.272	6.529	0.748	0.0112	0.9994	Papadopoulos and Hill
S	23	7.311	11.364	0.724	0.0171	0.9993	Zelinka and Glass
S	23	7.596	10.754	0.719	0.0377	0.9981	Zhang et al
H	25	7.323	6.738	0.671	0.0091	0.9998	Jalaludin et al
H	25	7.072	6.930	0.708	0.0120	0.9996	Jalaludin et al
H	24	6.227	7.026	0.764	0.0112	0.9998	Jakieła et al
H	25	8.000	7.520	0.701	0.0192	0.9993	Okoh and Skaar
H	30	5.332	13.413	0.867	0.0306	0.9987	Choong and Achmadi
T	30	6.646	4.273	0.783	0.0204	0.9996	Choong and Achmadi
T	30	5.569	7.097	0.825	0.0157	0.9997	Choong and Achmadi
T	30	6.428	8.691	0.839	0.0089	0.9999	Choong and Achmadi
T	30	5.667	7.474	0.847	0.0263	0.9992	Choong and Achmadi
T	30	6.245	5.319	0.775	0.0142	0.9997	Choong and Achmadi
T	30	6.316	5.425	0.803	0.0200	0.9995	Choong and Achmadi
T	30	5.432	9.312	0.844	0.0143	0.9997	Choong and Achmadi
T	30	6.462	7.425	0.779	0.0185	0.9995	Choong and Achmadi
T	30	5.877	6.874	0.822	0.0215	0.9994	Choong and Achmadi
T	30	5.591	7.185	0.831	0.0356	0.9983	Choong and Achmadi
T	30	5.837	5.427	0.801	0.0171	0.9996	Choong and Achmadi
T	30	6.323	5.457	0.772	0.0193	0.9995	Choong and Achmadi
T	30	5.493	7.976	0.859	0.0249	0.9992	Choong and Achmadi
T	30	5.643	10.279	0.853	0.0194	0.9995	Choong and Achmadi
T	30	4.834	20.049	0.916	0.0386	0.9984	Choong and Achmadi

The species classification "northern softwood", "northern hardwood", and "tropical wood" are represented by "S", "H", and "T" respectively. Tropical wood are primarily hardwood.

vector *RHS*. The subscripts n and $n+1$ represent the current step and the next step in Newton-Raphson method.

The element level entries of the Jacobian matrix of *AMATRX* are given by

$$\begin{aligned}\frac{\partial f_{ij}^e}{\partial h} = &\int_{\Omega^e}\left(\frac{\partial C_1}{\partial h}N_iN_j\right)\mathrm{d}V\ \dot{h}_j + \int_{\Omega^e} C_1N_iN_j\mathrm{d}V\left(\frac{\dot{h}_j}{\partial h}\right)+\\ &\int_{\Omega^e}\left[-\left(\frac{\partial D_{u1}}{\partial h}\frac{\partial N_i}{\partial x_1}\frac{\partial N_j}{\partial x_1}+\frac{\partial D_{u2}}{\partial h}\frac{\partial N_i}{\partial x_2}\frac{\partial N_j}{\partial x_2}+\frac{\partial D_{u3}}{\partial h}\frac{\partial N_i}{\partial x_3}\frac{\partial N_j}{\partial x_3}\right)\right]\mathrm{d}V\ h_j+\\ &\int_{\Omega^e}\left[-\left(D_{u1}\frac{\partial N_i}{\partial x_1}\frac{\partial N_j}{\partial x_1}+D_{u2}\frac{\partial N_i}{\partial x_2}\frac{\partial N_j}{\partial x_2}+D_{u3}\frac{\partial N_i}{\partial x_3}\frac{\partial N_j}{\partial x_3}\right)\right]\mathrm{d}V\end{aligned} \tag{14}$$

and the element level entries of *RHS* are given by

$$-f_{ij}^{e} = -\left(\int_{\Omega^e} C_1 N_i N_j \mathrm{d}V \ \dot{h}_j + \int_{\Omega^e} \left[-\left(D_{u1} \frac{\partial N_i}{\partial x_1} \frac{\partial N_j}{\partial x_1} + D_{u2} \frac{\partial N_i}{\partial x_2} \frac{\partial N_j}{\partial x_2} + D_{u3} \frac{\partial N_i}{\partial x_3} \frac{\partial N_j}{\partial x_3} \right) \right] \mathrm{d}V \ h_j \right) \tag{15}$$

For the rate term $\dot{\mathbf{h}}$, this work used a backward Euler time integration scheme, which is also the default time integration scheme in Abaqus/Standard. The backward Euler method is unconditionally stable, and large time increments are allowed when comparing with other conditionally stable time integration schemes. Specifically, one can rewrite the governing equation Eq. 12 by

$$\mathbf{M}\dot{\mathbf{h}} + \mathbf{K}\mathbf{h} \approx \mathbf{M}_{n+1} \frac{\mathbf{h}_{n+1} - \mathbf{h}_n}{\Delta t_{n+1}} + \mathbf{K}_{n+1}\mathbf{h}_{n+1} = \mathbf{0} \tag{16}$$

In which the subscripts n and $n+1$ here represent the previous time step and the current time step. One may notice that the incremental form of the governing equations should take the partial derivatives at the current time and that the matrices and the known term must be evaluated at the current time.

2.2.3 Identification methodology

Following implementation of the diffusion model in Abaqus, simulations are used to identify the permeability tensor parameters for a series of experimental data. The method is outlined here, using as example Perkowski et al (2017), which includes three different species with moisture transport in the longitudinal, radial, and tangential directions. In Perkowski et al (2017), nine (9) samples were prepared for each type of wood. In order to allow diffusion processes in a particular direction, the wood cube sample was sealed along four surfaces in each test. Fig. 2 shows a schematic with diffusion in the fiber direction. Although there are multiple tests in each direction for each species, an average of the data per direction was taken to avoid bias.

Experiments were conducted at 20°C, within a climate chamber where relative humidity was raised from 25% to 85%. To achieve this in the numerical simulation, a pre-defined field of 25% of relative humidity was assigned to the model and one surface was subjected to 85% relative humidity during the simulation. It is worth noting that a large gradient of moisture change on the surface can results in gradient errors in numerical simulation. Thus, a mesh gradient was used for the model shown in Fig. 2, with a gradually increasing time step for stability. The average specimen moisture content over time is give in Fig. 3, calculated by Eq. 17.

$$\bar{u} = \sum_{n=1}^{n_{el}} \frac{\int_{v^e} u dV}{V_{\text{total}}} \tag{17}$$

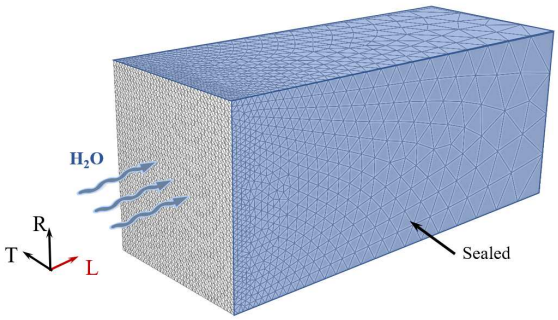

Fig. 2 3D geometry with mesh gradient of moisture diffusion in longitudinal direction

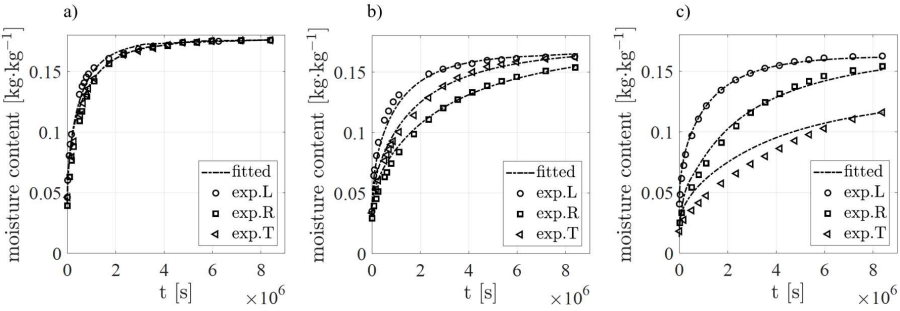

Fig. 3 The measured and calculated development of moisture profiles of a) pine; b) linden; c) oak

where n_{el} is the number of elements, V_{total} is the sample volume computed by summing of volume for each element, and u is obtained from the isotherm model using average parameters.

Temperature dependent permeability parameters were also calibrated and validated. In Hukka (1999), radial direction of Scots pine and Norway spruce were tested at 20°C, 50°C, and 80°C. In the simulation, permeability parameters of $D_{u2} = 6.0 \times 10^{-11}$ ($m^2 \cdot s^{-1}$) and $E_{ad} = 3097$ ($mol \cdot J^{-1}$) for Norway spruce and $D_{u2} = 6.0 \times 10^{-11}$ ($m^2 \cdot s^{-1}$) and $E_{ad} = 2675$ ($mol \cdot J^{-1}$) for Scots pine were identified through modeling of the 20°C and 50°C experiments. Then, those parameters were applied to predict 80°C moisture transport behaviors. Fig. 4 and 5 show how well the model captures the temperature dependent diffusion process. It can be seen that the boundary values track the data well over time, and the mid-point only slight deviates from the experimental trends.

Glulam timber experiments were also collected if the moisture transport direction was parallel to the glued surface. In Angst and Malo (2012), Norway spruce was used to test the moisture diffusion in the radial direction. It is noted that in reality, the surfaces exposed to the environment are not equal to the relative humidity outside, which is not the case for the simulation. To address this inconsistency, a surface mesh is modelled to mimic the real situation.

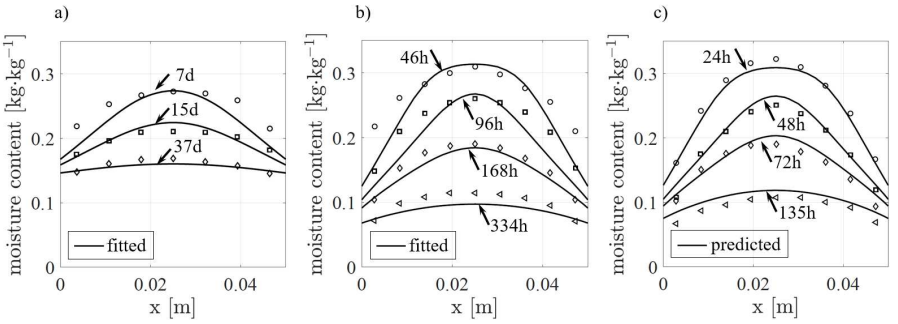

Fig. 4 The measured moisture profiles in radial direction of Scot's pine with a) fitted moisture development at 20°C; b) fitted moisture development at 50°C; c) predicted moisture development at 80°C

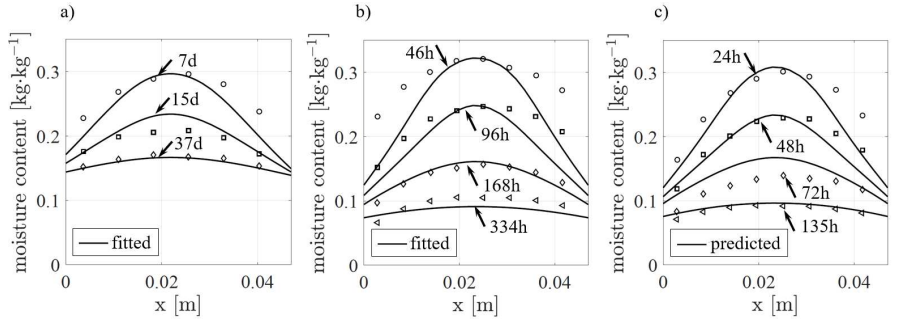

Fig. 5 The measured moisture profiles in radial direction of Norway spruce with a) fitted moisture development at 20°C; b) fitted moisture development at 50°C; c) predicted moisture development at 80°C

Thus, in Fig. 6 the surface moisture content does not start at the same value in different time steps.

To quantify the quality of fitting and prediction for diffusion process, unbiased least square method was also implied to compare between the experimental and numerical results as reference to Table 4.

2.2.4 Database of moisture transport parameters

The database for moisture permeability parameters for various species in all three directions was created as shown in Table 2. The diffusion parameter for wood in the fiber direction (longitudinal) is found to be around an order of magnitude larger than the radial or tangential directions. This may be due to denser membranes in radial and tangential direction, which means there are fewer open areas in series allowing bound water to jump from one cellulose molecule to another. Although the permeability in the radial and tangential directions are similar, diffusion in the radial direction is generally larger, a result of more ray cells in parallel with diffusion (Hawley, 1931). Comparing general wood categorization, softwood has higher permeability than hardwood;

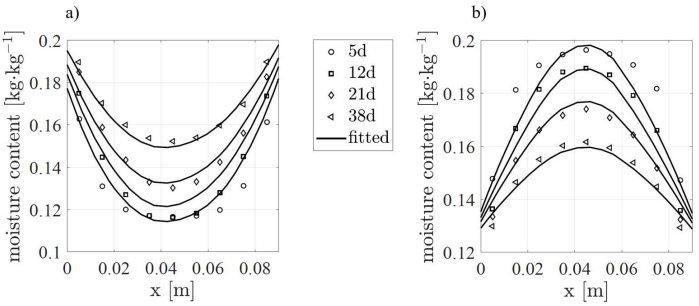

Fig. 6 The measured moisture profiles consisting of six laminates of Norway spruce with a) fitted moisture gradient of adsorption; b) fitted moisture gradient of desorption

Table 2 Experiment conditions and fitted parameters for moisture diffusion of different species

Direction	T (°C)	Δh (%)	Time (d)	Permeability (m/s^2)	Source
L	23	60	115	2.17E-10	Eitelberger et al
L	30	25	1	5.88E-10	Droin et al
L	20	60	100	3.90E-10	Perkowski et al
L	20	60	100	1.90E-10	Perkowski et al
L	20	60	100	2.01E-10	Perkowski et al
L	25	32	0.5	6.65E-10	Amer et al
L	25	32	0.5	3.90E-10	Amer et al
R	20	35	26	6.00E-11	Hukka
R	23	60	89	5.00E-11	Eitelberger et al
R	20	60	16	5.00E-11	Perkowski et al
R	20	35	37	6.00E-11	Hukka
R	43	63	16	2.93E-11	Simpson
R	20	60	100	1.00E-11	Perkowski et al
R	20	60	100	9.50E-12	Perkowski et al
R	25	32	0.5	5.00E-11	Amer et al
R	25	32	0.5	5.00E-11	Amer et al
T	20	40	38	6.00E-11	Jönsson
T	23	60	82	4.17E-11	Eitelberger et al
T	20	60	38	3.25E-11	Angst and Malo
T	20	60	100	5.00E-11	Perkowski et al
T	20	60	100	5.00E-12	Perkowski et al
T	20	60	100	1.23E-11	Perkowski et al
T	25	32	0.5	5.00E-11	Amer et al
T	25	32	0.5	5.00E-11	Amer et al

this can be seen in Fig. 7 and in Table. 3. However, as few softwood species were included (due to scarcity of relevant experimental data in the literature), this conclusion is not statistically validated, and more data should be collected. In Table 3, one can observe that diffusion behaviors between species provide a large variance even in the same category, as oppose to the narrow variation of the sorption isotherm curve.

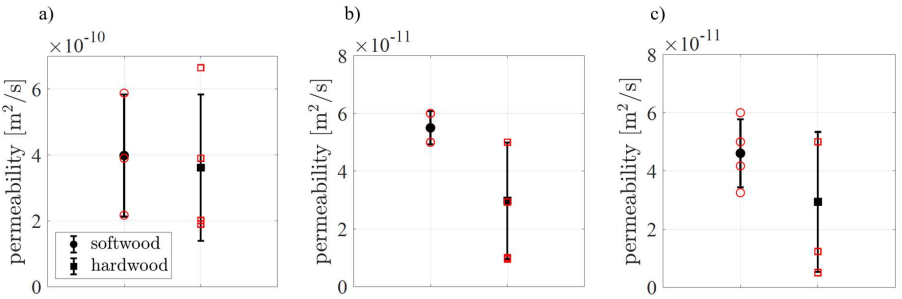

Fig. 7 Mean and standard deviation of moisture permeability for hardwood and softwood in a) longitudinal direction; b) radial direction; c) tangential direction; red symbols are individual diffusion values

Table 3 Statistical analysis of permeability for softwood and hardwood

	$D_{ui,S}$			$D_{ui,H}$			Avg. Ratio
Dir.	μ ($\frac{pm}{s^2}$)	σ ($\frac{pm}{s^2}$)	C_v (%)	μ ($\frac{pm}{s^2}$)	σ ($\frac{pm}{s^2}$)	C_v (%)	$\frac{D_S}{D_H}$
L	398	186	46.7	377	2.22	58.9	1.06
R	55	5	10.5	41	20.1	49.0	1.34
T	46.1	11.7	25.4	37.7	18.9	50.1	1.22

μ, mean value; σ, standard deviation; C_v, coefficient of variation; i = 1, 2, 3 represents for longitudinal, radial and tangential direction.

3 Prediction and Discussion

The database can now be used for prediction of wood moisture transport behavior for engineered wood commonly used in mass timber buildings. To validate the database for moisture permeability, identified parameters were used to predicted the diffusion process of both one-dimensional and two-dimensional timber structural elements.

3.1 Glulam

In the work of Franke et al (2016), softwood glulam specimens were cut to 200×200×200 mm. The experiment was conducted under 20°C and 65% relative humidity for longitudinal, radial, and tangential directions. Specimens were loaded under 95% relative humidity lasting a period of 12 months. To guarantee the diffusion transport along three material axes respectively in each test, the side surfaces were sealed. The isotherm parameters are: $X_m = 7.02$, $C = 7.63$, and $K = 0.75$. Diffusion parameters were taken from the average values of all northern softwoods (see Table 3). The predicted behavior was compared and plotted together with experimental data as shown in Fig. 8. The prediction captures well the overall moisture diffusion for glulam in three directions as time goes on, similar to the solid wood predictions shown in Figs. 4 and 5. The quantitative analysis for the goodness of the prediction is shown in Table 4.

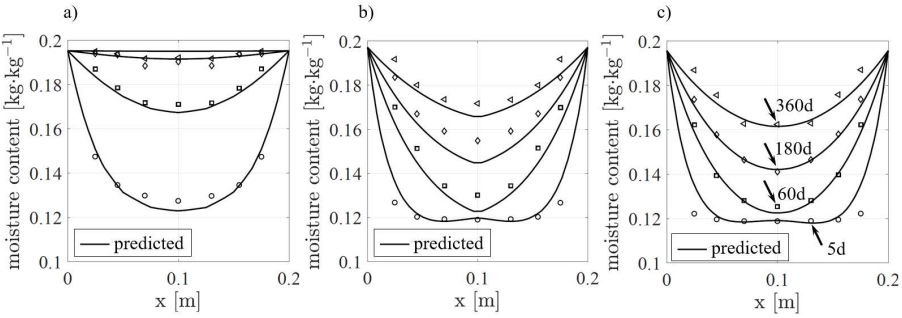

Fig. 8 The measured moisture profiles with prediction in a) L direction; b) R direction; T direction ; the x-axis is the distance of the tested surface to one surface exposed to the environment

3.2 Laminated panel

This diffusion model can also be applied to predict timber panel mass transport. Three panel types were tested in Tripathi and Rice (2019). The first panel type consisted of three layers of Eastern red spruce (3-spruce); the second panel consisted of red spruce as face layer and laminated strand lumber (LSL) in the core layer (spruce-LSL-spruce); the third panel consisted of LSL as the face layers and a red spruce the core layer (LSL-spruce-LSL). Tests were conducted in a temperature and moisture controlled chamber, with one face exposed to a dry and cool environment at 40% relative humidity and the other to a warm and moist environment with 99% of relative humidity. It is assumed here that temperature effects are negligible for moisture diffusion. The adhesive used in the test had high permeability; in combination with the thinness of the layers, the adhesive may be ignored in the simulation (Hayashi et al, 1993).

It is not discussed in the paper how the panels were cut and assembled, nor were photos included. It cannot then be directly known whether the out-of-plane diffusion was tangential or radial. In addition, LSL experiments were not found to directly fit the permeability of strand lumber. Thus, the direction of spruce transport and LSL parameter should be determined before predicting the panel moisture transport. To accomplish this, one spruce-LSL-spruce experimental data set was used, simulating permeability using both radial and tangential parameters to determine which direction seemed most likely. From this it was seen that it was most likely radial diffusion occurring in the spruce, as the tangential parameters consistently underestimated the moisture content.

Following this, the same experiment was used to fit the LSL permeability, assuming now that spruce was radial diffusion. The final diffusion parameters for best fit were found to be: $D_{u2,spruce} = 6.27{\times}10^{-11}$ $\mathrm{m^2{\cdot}s^{-1}}$ and $D_{u2,LSL}$ $2.5{\times}10^{-11} = \mathrm{m^2{\cdot}s^{-1}}$. It might be noted that the relatively small permeability value of LSL proves it capable of resisting moisture diffusion as a structural material. Figure 9a shows that the fitted parameters are reasonable for this data.

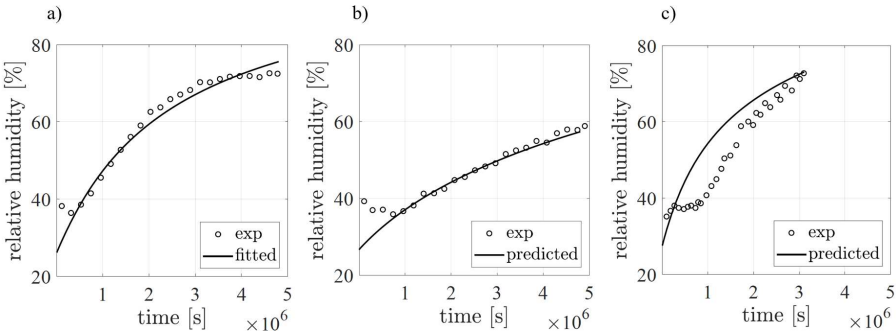

Fig. 9 The measured relative humidity of a) spruce-LSL-spruce with fitted curve; b) LSL-spruce-LSL with predicted curve; c) 3-spruce with predicted curve

Following this parameter identification, the tests of LSL-spruce-LSL and 3-spruce moisture transport behavior were predicted using identified values. The results are shown in Fig. 9. The weighted least square method was exerted here for quantifying the goodness of the prediction as presented in Table 4.

It can be seen that, although the model follows well the overall moisture transport process of the LSL-spruce-LSL specimen, it could not capture the 3-spruce specimen diffusion. This may be due to the inconsistent behavior of the 3-spruce experimental data over time - it can be clearly seen that the trend is not consistent, which is unexpected for such experimental setup, and in direct contrast to the other two specimens. This variation in data may be due to the different initial conditions of these panels, as outlined in Tripathi and Rice (2019), which shows the 3-spruce specimen starting at a lower MC than the other two. Regardless, the authors concluded that the variation does not discount the conclusions regarding the proposed model.

3.3 CLT roof panel

As seen, the developed orthotropic moisture diffusion model reasonably predicts lab diffusion experiments. However, it is also important to understand the validity of the model in *in-situ* conditions. For this test, data was supplied from tests of in-situ monitoring of a new mass timber building by Kordziel et al (2019). Kordziel et al (2020) performed additional lab testing to determine material properties for computational prediction of said monitoring, with good results. In this study the authors attempt to predict the Kordziel et al (2019) using only those parameters identified in the preceding sections.

The observed CLT roof panel was 139 mm thick and consisted of four layers of wood from the spruce-pine-fir (SPF) species group and one layer of Douglas-fir (DF). Layer 1 refers to the topmost layer exposed to the elements, and layer 5 is the innermost panel, which experienced conditioned air once the structure was sealed. Layer 1 was not modeled, as the authors note the sensors were not fully sealed and became directly exposed to the rain, invalidating their results for diffusion analysis.

Table 4 Solid wood and laminated timber fitting and prediction

Type	Species	Direction	ω (%)	r^2	Source
F	Pine	L	9.28	0.9999	Perkowski et al
F	Pine	R	10.56	0.9999	Perkowski et al
F	Pine	T	9.63	0.9999	Perkowski et al
F	Linden	L	9.06	0.9999	Perkowski et al
F	Linden	R	14.94	0.9997	Perkowski et al
F	Linden	T	14.87	0.9997	Perkowski et al
F	Oak	L	8.17	0.9999	Perkowski et al
F	Oak	R	19.74	0.9995	Perkowski et al
F	Oak	T	60.59	0.9948	Perkowski et al
F	Pine	R	12.22	0.9995	Hukka
F	Pine	R	36.91	0.9965	Hukka
P	Pine	R	24.83	0.9982	Hukka
F	Spruce	R	10.85	0.9995	Hukka
F	Spruce	R	36.94	0.9964	Hukka
P	Spruce	R	53.88	0.9984	Hukka
F	Spruce	R	10.82	0.9995	Hukka
F	Spruce	R	8.59	0.9997	Hukka
P	Spruce	L	3.53	0.9999	Franke et al
P	Spruce	R	8.56	0.9998	Franke et al
P	Spruce	T	4.32	0.9999	Franke et al
F	Spruce-LSL-Spruce	R	18.93	0.9995	Tripathi and Rice
P	LSL-Spruce-LSL	R	18.35	0.9995	Tripathi and Rice
P	3-Spruce	R	79.23	0.9980	Tripathi and Rice

F represents fitted results, P represents predicted results.

Sensors were installed in each layer to monitor the moisture content. The initial moisture content for layer 1-5 are 32%, 19%, 20%, 18%, and 16% respectively. Kordziel et al (2020) presented photos of the layup of the panel; radial softwood diffusion parameters from the database were used based on this information. The sorption isotherm parameters for softwood were also used. Two tests were run, representing the upper-most and lower-most bounds of the database predictions. The results of each layer with respect to the measured data is displayed in Fig. 10, with the shaded region representing the range of predictions using the database data.

One can observe that the prediction range overall follows the trend of test data. However, the prediction underestimated the moisture content of layers 2 through 4, while overestimated layer 5 (exposed to the interior of the structure). Moreover, the values of upper bound and lower bound of layer 2 and layer 3 provide a wide envelope which increase the uncertainty of the prediction. These results make clear the current database of parameters must be expanded for accurate long-term prediction of realistic conditions.

4 Conclusions

An orthotropic hygroscopic model for wood is developed with application to real projects. A database for sorption isotherms was created and the GAB model was used to fit parameters. A similar database of moisture permeability

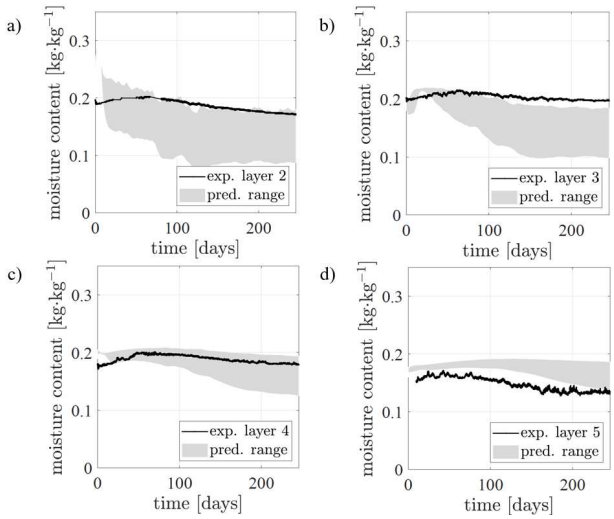

Fig. 10 The measured moisture content of CLT roof panel with prediction range of a) layer 2; b) layer 3; c) layer 4; d) layer 5

parameters for various wood species including hardwood and softwood was formed based on numerical simulation.

It was found that

- The isotherm parameters exhibited lower variance than expected. In particular, there was no discernible trend among species categorization such as hardwood/softwood or tropical-grown woods. Moreover, the variation to the average curve was minimal between adsorption and desorption, supporting the assumption of a single curve in both directions for computational modelling.
- In contrast, moisture diffusion variation was high between species, with softwood exhibiting higher permeability compared with hardwoods. This is intuitive, as hardwoods species are generally higher in density. The orthotropy of the diffusion parameters is also expected, with radial and tangential directions being an order of magnitude greater than the longitudinal directions.
- A model which utilizes the database parameters predicts well the moisture transport of wood in laboratory conditions. Both solid timber as well as laminated timber show great agreement with experimental data over time. Moreover, prediction through the cross-section of the material is excellent despite minimal data available. This approach may then be used for further consideration of moisture movement across lamination and adhesion layers.
- The database also reasonably predicts CLT moisture diffusion under real conditions. Though the range of prediction uncertainty is wide, it is meaningful for construction and structural engineering purposes, and may be used for moisture-dependent behaviors such as mechanosorptive creep, to predict realistic building behavior over long time scales.

- Drawbacks of this method include limitations in the number of available diffusion experiments. Furthermore, the effect of adhesives is not considered, which may impact the applicability to laminated elements. This method also uses a simplified diffusion approach, considering only diffusion of bound liquid water. Inclusion of the vapor phase may improve results for a greater range of moisture content.

In the future, the database for both sorption isotherm and diffusion should be expanded, which the authors expect will allow for further refinement of the model (e.g. specifying a single species group such as spruce-pine-fir, rather than all softwood values). The adhesion properties might also be directly simulated to improve overall validation for engineered wood products.

Appendix A Weighted least square method

In the isotherm database, data points are not necessarily distributed evenly along x-axis (relative humidity). Thus, the data for each curve was divided by intervals of equal size. Noted that if the data points are almost equally spaced, it is not necessary to divide into intervals or add the weight. The number of intervals, n, was defined such that each interval has a similar number of data points, m_i, where i = 1, 2, ...n. To eliminate human bias, the same weight was assigned to each interval. This is achieved by considering the statistical weights w_i of the individual data points in each interval to be inversely proportional to the number m_i of data points in that interval and $\sum_{i=1}^{n} w_i = 1$. Then $\bar{w} = \sum_{i=1}^{n} \frac{1}{m_i}$ and $w_i = \frac{1}{m_i \bar{w}}$ where the w_i is the i^{th} interval weight

Once the equal weighted interval was obtained, the standard error s of the prediction model is defined as follows:

$$s = \sqrt{\frac{N}{N-p} \sum_{i=1}^{n} w_i \sum_{j=1}^{m} (Y_{ij} - y_{ij})^2} \tag{A1}$$

where y_{ij} are the measured isotherm data; Y_{ij} are the corresponding GAB predictions; N is the number of all data points in the database; p is the number of input parameters of the model ($p = 3$ for GAB model). $\epsilon_{ij} = y_{ij} - Y_{ij}$ computes the arithmetic difference between the measured points and predictions.

Next, the least square estimation of unknown parameters is found by minimizing Eq. A1 for each individual data curve and the whole database, respectively. Once parameters are identified, it is possible to evaluate the fit and prediction quality. Two statistical indicators are introduced. The first is the coefficient of variation of the regression errors ω (%) which characterizes the ratio of the scatter band width to the data mean $\omega = \frac{s}{\bar{y}}$ and $\bar{y} = \frac{\bar{w}}{n} \sum_{i=1}^{n} w_i \sum_{j=1}^{m_i} y_{ij}$ where $\bar{y}$ represents the weighted mean value of measured points in the database. The smaller the ω is, the more accurate the fitting results.

The second term is the coefficient of determination r^2, which specifies the ratio of the scatter band width to the overall spread of data and designates what percentage of data variation is accounted for by the model response as $r^2 = 1 - \frac{s^2}{\bar{s}^2}$.

$$\bar{s} = \sqrt{\frac{N}{N-1} \sum_{i=1}^{n} w_i \sum_{j=1}^{m} (Y_{ij} - \bar{y})^2} \tag{A2}$$

A value of $r^2 = 1$ indicates the prediction is closer to measured points.

Appendix B Expanded derivation of the finite element implementation

The primary field, relative humidity h, in an infinitesimal control volume Ω with the boundary subjected to the inflow/outflow of mass Γ_h, the moisture mass balance equation reads

$$\int_{\Omega} \frac{\partial u}{\partial t} dV = \int_{\Gamma_h} q_h dA \tag{B3}$$

where the rate term (or capacity term) $\partial u/\partial t = (\partial u/\partial h)(\partial h/\partial t)$, the diffusion flux density of water mass per unit time $q_h = -\mathbf{J} \cdot \mathbf{n}$, $\mathbf{J}$ is the mass flux density vector per unit time, $\mathbf{n}$ is the normal vector of the boundary where the flux passes through. The flux density vector per unit time $\mathbf{J}$ can be associated with the relative humidity gradient $\boldsymbol{\nabla} h$ by an equivalent Darcy's law $\mathbf{J} = -\mathbf{D_u}\, \boldsymbol{\nabla} h$ where $\mathbf{D_u}$ is the orthotropic moisture permeability matrix.

To derive the finite element formulation, we need to find the weak form of the governing balance equations mentioned above. For boundary flux term, by using the divergence theorem:

$$\int_{\Gamma_h} q_h dA = -\int_{\Gamma_h} \mathbf{J} \cdot \mathbf{n} dA = -\int_{\Omega} \boldsymbol{\nabla} \cdot \mathbf{J} dV \tag{B4}$$

Substituting Eq. B4 into Eq. B3 yields

$$\int_{\Omega} \left(\frac{\partial u}{\partial t} + \boldsymbol{\nabla} \cdot \mathbf{J} \right) dV = 0 \tag{B5}$$

By multiplying arbitrary test functions δh to Eq. B5, one obtains

$$\int_{\Omega} \left(\delta h \frac{\partial u}{\partial t} + \delta \boldsymbol{\nabla} h \boldsymbol{\nabla} \cdot \mathbf{J} \right) dV = 0 \tag{B6}$$

After integral by parts, Eq. B6 becomes

$$\int_{\Omega} \left(\delta h \frac{\partial u}{\partial t} + \delta \boldsymbol{\nabla} h \cdot \mathbf{J} \right) dV + \int_{\Gamma_h} \delta h q_h dA = 0 \tag{B7}$$

The temporal discretization of rate terms uses the Backward Euler scheme:

$$\frac{\partial u}{\partial t} = \frac{\partial u}{\partial t}\Big|_{t+\Delta t} = \frac{u_{t+\Delta t} - u_t}{\Delta t} \tag{B8}$$

where the subscript t denotes for the values in the current time step, $t+\Delta t$ denotes for the values in the next time step.

The spatial discretization of the primary field is selected to be consistent with classical Galerkin FEM, which reads:

$$h = \sum_{i=1}^{n_{node}} N_i h_i = N_i h_i;\ \delta h = \sum_{i=1}^{n_{node}} N_i \delta h_i = N_i \delta h_i;\ \boldsymbol{\nabla} h = \sum_{i=1}^{n_{node}} \sum_{j=1}^{n_{dim}} \frac{\partial N_i}{\partial x_j} h_i = \frac{\partial N_i}{\partial x_j} h_i \tag{B9}$$

where n_{node} is number of nodes for the element, h_i, and δh_i are nodal relative humidity and associated nodal testing function at the i^{th} node, respectively, N_i is the shape function at the i^{th} node, $\partial N_i/\partial x_j$ is the first derivative of the shape function at the i^{th} node with respect to j^{th} dimension. The element-wise Eq. B7 can be discretized as

$$\sum_{i=1}^{n_{node}} \sum_{j=1}^{n_{node}} \left\{ \int_{\Omega^e} \left[N_i \delta h_i N_j \dot{u}_j + \sum_{k=1}^{3} \sum_{l=1}^{3} \frac{\partial N_i}{\partial x_k} \delta h_i \left(D_{ul} \frac{\partial N_j}{\partial x_l} h_j \right) \right] dV - \int_{\Gamma_h} N_i \delta h_i q_h dA \right\} = 0 \tag{B10}$$

where Ω^e denotes the element domain, D_{ul} denotes the diffusivity in l^{th} dimension. By using the Einstein notation, the summations $\sum_{i=1}^{n_{node}}$, $\sum_{i=j}^{n_{node}}$, $\sum_{k=1}^{3}$, $\sum_{l=1}^{3}$ will be simplified in equations below. Since the variational field δh can be arbitrarily chosen, the term in the biggest braces of Eq. B10 should equal to 0, which makes:

$$\int_{\Omega^e} \left[N_j \dot{u}_j + \frac{\partial N_i}{\partial x_k} \left(D_{ul} \frac{\partial N_j}{\partial x_l} h_j \right) \right] dV - \int_{\Gamma_h} q_h dA = 0 \tag{B11}$$

Denotes Eq. B11 as function f, for the situation $f = 0$, use Newton-Raphson method to linearize the equation with the form: $f(x_{n+1}) = f(x_n) + \frac{\partial f(x_n)}{\partial x} \Delta x + H.O.T$ (high order terms, neglected)

$$f(h_{n+1}) \approx f(h_n) + \frac{\partial f}{\partial h} \Delta h = 0 \tag{B12}$$

rearranging the equations yields

$$\frac{\partial f}{\partial h} \Delta h = -f(h_n) \tag{B13}$$

where the subscript n and $n+1$ denotes the current and the next Newton step, respectively. The matrix on the left hand side is the Jacobian (or tangent stiffness) matrix (AMATRX in user subroutines). The vector on the right hand side is called residual (RHS in user subroutines).

Substituting the discritized rate term in Eq. (B11) yields

$$f = \int_{\Omega^e} N_j \left(\frac{\partial u}{\partial h} \frac{h_{j,t+\Delta t} - h_{j,t}}{\Delta t} \right) dV + \int_{\Omega e} \frac{\partial N_i}{\partial x_k} D_{ul} \frac{\partial N_j}{\partial x_l} h_j dV \tag{B14}$$

For the variables that depend on humidity, since $h_{t+\Delta t} = N_j h_{j,t+\Delta t}$, the variation with respect to the nodal humidity values can be written:

$$\frac{\partial f}{\partial h_{i,t+\Delta t}} = \frac{\partial f}{\partial h_{t+\Delta t}} \frac{\partial (N_j h_{j,t+\Delta t})}{\partial h_{i,t+\Delta t}} = \frac{\partial f}{\partial h_{t+\Delta t}} N_j \tag{B15}$$

For the partial derivative of f with respect to h, the rate/capacity term reads:

$$\begin{aligned} &\int_{\Omega^e} \frac{\partial}{\partial h_{j,t+\Delta t}} \left[N_j \left(\frac{\partial u}{\partial h} \frac{h_{j,t+\Delta t} - h_{j,t}}{\Delta t} \right) \right] dV \\ &= \int_{\Omega^e} N_i N_j \left[\frac{\partial^2 u}{\partial h_{t+\Delta t}^2} \left(\frac{h_{j,t+\Delta t} - h_{j,t}}{\Delta t} \right) + \frac{\partial u}{\partial h_{t+\Delta t}} \frac{1}{\Delta t} \right] dV \end{aligned} \tag{B16}$$

the gradient term:

$$\begin{aligned} &\int_{\Omega e} \frac{\partial}{\partial h_{j,t+\Delta t}} \left[\frac{\partial N_i}{\partial x_k} D_{ul} \frac{\partial N_j}{\partial x_l} h_j \right] dV \\ &= \int_{\Omega^e} \left[\frac{\partial N_i}{\partial x_k} \left(N_j \frac{\partial D_{ul}}{\partial h_{j,t+\Delta t}} \right) \frac{\partial N_j}{\partial x_l} h_j + \frac{\partial N_i}{\partial x_k} D_{ul} \frac{\partial N_j}{\partial x_l} \right] dV \end{aligned} \tag{B17}$$

Combining Eq.B16 and B17, one gets:

$$\begin{aligned} \frac{\partial f}{\partial h_{j,t+\Delta t}} = \int_{\Omega^e} \Bigg\{ & N_i N_j \left[\frac{\partial^2 u}{\partial h_{t+\Delta t}^2} \left(\frac{h_{j,t+\Delta t} - h_{j,t}}{\Delta t} \right) + \frac{\partial u}{\partial h_{t+\Delta t}} \frac{1}{\Delta t} \right] \\ & + \frac{\partial N_i}{\partial x_k} \left(N_j \frac{\partial D_{ul}}{\partial h_{j,t+\Delta t}} \right) \frac{\partial N_j}{\partial x_l} h_j + \frac{\partial N_i}{\partial x_k} D_{ul} \frac{\partial N_j}{\partial x_l} \Bigg\} dV \end{aligned} \tag{B18}$$

Gauss quadrature is a prevalent approach for numerical integration in most finite element methods, it required the space mapping from the parent domain $\boldsymbol{\xi}$ to the physical domain $\mathbf{x}$, however, this falls in conventional finite element scope and will not be derived here; for details, one may refer to Belytschko et al (2000).

References

Abbasion S, Carmeliet J, Gilani MS, et al (2015) A hygrothermo-mechanical model for wood: part a. poroelastic formulation and validation with neutron

imaging. Holzforschung 69(7):825–837. https://doi.org/https://doi.org/10.1515/hf-2014-0189

Abrahamsen R (2017) Mjøstårnet-construction of an 81 m tall timber building. International House Forum

Afshari Z, Malek S (2022) Moisture transport in laminated wood and bamboo composites bonded with thin adhesive layers–a numerical study. Construction and Building Materials 340:127,597. https://doi.org/https://doi.org/10.1016/j.conbuildmat.2022.127597

Amer M, Kabouchi B, Rahouti M, et al (2020) Experimental study of the linear diffusion of water in clonal eucalyptus wood. International Journal of Thermophysics 41(10):1–17. https://doi.org/https://doi.org/10.1007/s10765-020-02723-7

Angst V, Malo KA (2012) The effect of climate variations on glulam—an experimental study. European Journal of Wood and Wood Products 70(5):603–613. https://doi.org/https://doi.org/10.1007/s00107-012-0594-y

Autengruber M, Lukacevic M, Füssl J (2020) Finite-element-based moisture transport model for wood including free water above the fiber saturation point. International Journal of Heat and Mass Transfer 161:120,228. https://doi.org/https://doi.org/10.1016/j.ijheatmasstransfer.2020.120228

Baker WJ (1956) How wood dries. Forest Product Laboratory

Bažant ZP, Li GH (2008) Unbiased statistical comparison of creep and shrinkage prediction models. ACI materials Journal 105(6):610–621. https://doi.org/https://doi.org/10.14359/20203

Bažant Z, Najjar L (1972) Nonlinear water diffusion in nonsaturated concrete. Matériaux et Construction 5(1):3–20. https://doi.org/https://doi.org/10.1007/BF02479073

Belytschko T, Liu W, Moran B (2000) Nonlinear finite elements for continua and structures. John Wiley and Sons, New York

Borrega M, Kärenlampi PP (2011) Cell wall porosity in norway spruce wood as affected by high-temperature drying. Wood and Fiber Science 43(2):206–214

Brunauer S, Emmett PH, Teller E (1938) Adsorption of gases in multimolecular layers. Journal of the American chemical society 60(2):309–319

Chiniforush A, Akbarnezhad A, Valipour H, et al (2019) Moisture and temperature induced swelling/shrinkage of softwood and hardwood glulam and lvl: An experimental study. Construction and Building Materials 207:70–83.

https://doi.org/https://doi.org/10.1016/j.conbuildmat.2019.02.114

Choong ET, Achmadi SS (1991) Effect of extractives on moisture sorption and shrinkage in tropical woods. Wood and Fiber science pp 185–196

Dent R (1977) A multilayer theory for gas sorption: Part i: sorption of a single gas. Textile Research Journal 47(2):145–152. https://doi.org/https://doi.org/10.1177/004051757704700 21

Di Luzio G, Cusatis G (2009) Hygro-thermo-chemical modeling of high performance concrete. i: Theory. Cement and Concrete composites 31(5):301–308. https://doi.org/https://doi.org/10.1016/j.cemconcomp.2009.02.015

Droin A, Taverdet J, Vergnaud J (1988) Modeling the kinetics of moisture adsorption by wood. Wood Science and Technology 22(1):11–20. https://doi.org/https://doi.org/10.1007/BF00353224

Eitelberger J, Hofstetter K, Dvinskikh SV (2011) A multi-scale approach for simulation of transient moisture transport processes in wood below the fiber saturation point. Composites Science and Technology 71(15):1727–1738. https://doi.org/https://doi.org/10.1016/j.compscitech.2011.08.004

Fernandez A, Komp J, Peronto J (2020) Ascent-challenges and advances of tall mass timber construction. International Journal of High-Rise Buildings 9(3):235–244. https://doi.org/https://doi.org/10.21022/IJHRB.2020.9.3.235

Franke B, Franke S, Schiere M, et al (2016) Moisture diffusion in wood–experimental and numerical investigations. In: World Conference on Timber Engineering, https://doi.org/10.24451/arbor.7304

Fredriksson M, Thybring EE (2018) Scanning or desorption isotherms? characterising sorption hysteresis of wood. Cellulose 25(8):4477–4485. https://doi.org/https://doi.org/10.1007/s10570-018-1898-9

Gezici-Koç Ö, Erich SJ, Huinink HP, et al (2017) Bound and free water distribution in wood during water uptake and drying as measured by 1d magnetic resonance imaging. Cellulose 24(2):535–553. https://doi.org/https://doi.org/10.1007/s10570-016-1173-x

Hawley LF (1931) Wood-liquid relations. 248, US Department of Agriculture

Hayashi S, Ishikawa N, Giordano C (1993) High moisture permeability polyurethane for textile applications. Journal of Coated Fabrics 23(1):74–83. https://doi.org/https://doi.org/10.1177/152808379302300110

Hill CA, Ramsay J, Keating B, et al (2012) The water vapour sorption properties of thermally modified and densified wood. Journal of Materials Science 47(7):3191–3197. https://doi.org/https://doi.org/10.1007/s10853-011-6154-8

Hoffmeyer P, Davidson R (1989) Mechano-sorptive creep mechanism of wood in compression and bending. Wood Science and Technology 23(3):215–227. https://doi.org/https://doi.org/10.1007/BF00367735

Holzer SM, Loferski JR, Dillard DA (1989) A review of creep in wood: concepts relevant to develop long-term behavior predictions for wood structures. Wood and Fiber Science pp 376–392

Hozjan T, Svensson S (2011) Theoretical analysis of moisture transport in wood as an open porous hygroscopic material. Holzforschung 65(1):97–102. https://doi.org/https://doi.org/10.1515/hf.2010.122

Hukka A (1999) The effective diffusion coefficient and mass transfer coefficient of nordic softwoods as calculated from direct drying experiments. De Gruyter 53(5):534–540. https://doi.org/doi:10.1515/HF.1999.088

Hunt DG (1999) A unified approach to creep of wood. Proceedings of the Royal Society of London Series A: Mathematical, Physical and Engineering Sciences 455(1991):4077–4095. https://doi.org/https://doi.org/10.1098/rspa.1999.0491

Jakieła S, Bratasz Ł, Kozłowski R (2008) Numerical modelling of moisture movement and related stress field in lime wood subjected to changing climate conditions. Wood Science and Technology 42(1):21–37. https://doi.org/https://doi.org/10.1007/s00226-007-0138-5

Jalaludin Z, Hill CA, Samsi HW, et al (2010) Analysis of water vapour sorption of oleo-thermal modified wood of acacia mangium and endospermum malaccense by a parallel exponential kinetics model and according to the hailwood-horrobin model. De Gruyter 64(6):763–770. https://doi.org/doi:10.1515/hf.2010.100

Jönsson J (2004) Internal stresses in the cross-grain direction in glulam induced by climate variations. De Gruyter 58(2):154–159. https://doi.org/doi:10.1515/HF.2004.023

Kaymak-Ertekin F, Sultanoğlu M (2001) Moisture sorption isotherm characteristics of peppers. Journal of food engineering 47(3):225–231. https://doi.org/https://doi.org/10.1016/S0260-8774(00)00120-5

Kordziel S, Pei S, Glass SV, et al (2019) Structure moisture monitoring of an 8-story mass timber building in the pacific northwest. Journal of Architectural Engineering 25 (4) 14 p 25(4). https://doi.org/https://doi.org/10.1061/(ASCE)AE.1943-5568.0000367

Kordziel S, Glass SV, Boardman CR, et al (2020) Hygrothermal characterization and modeling of cross-laminated timber in the building envelope. Building and Environment 177:106,866. https://doi.org/https://doi.org/10.1016/j.buildenv.2020.106866

Kremer P, Symmons M (2015) Mass timber construction as an alternative to concrete and steel in the australia building industry: a pestel evaluation of the potential. International Wood Products Journal 6(3):138–147. https://doi.org/https://doi.org/10.1179/2042645315Y.0000000010

Krupińska B, Strømmen I, Pakowski Z, et al (2007) Modeling of sorption isotherms of various kinds of wood at different temperature conditions. Drying Technology 25(9):1463–1470. https://doi.org/https://doi.org/10.1080/07373930701537062

Lehne J, Preston F (2018) Making concrete change: Innovation in low-carbon cement and concrete. Tech. rep., Chatham House

Merakeb S (2006) Modélisation des structures en bois en environnement variable. Université de Limoges 46

Mukudai J, Yata S (1986) Modeling and simulation of viscoelastic behavior (tensile strain) of wood under moisture change. Wood Science and Technology 20(4):335–348. https://doi.org/https://doi.org/10.1007/BF00351586

Nakajima S, Sakabe Y, Kimoto S, et al (2020) Deterioration of clt under humid and dry cyclic climate. In: XV International Conference on Durability of Building Materials and Components (DBMC 2020), https://doi.org/10.23967/dbmc.2020.030

Okoh KI, Skaar C (1980) Moisture sorption isotherms of the wood and inner bark of ten southern us hardwoods. Wood and Fiber Science pp 98–111

Osborne L, Dagenais C, Bénichou N (2012) Preliminary clt fire resistance testing report. Point-Claire, Canada: Advanced Building Systems–Serviceability and Fire Group

Oswin C (1946) The kinetics of package life. iii. the isotherm. Journal of the Society of Chemical Industry 65(12):419–421. https://doi.org/https://doi.org/10.1002/jctb.5000651216

Pang SJ, Jeong GY (2020) Swelling and shrinkage behaviors of cross-laminated timber made of different species with various lamina thickness and combinations. Construction and Building Materials 240:117,924. https://doi.org/https://doi.org/10.1016/j.conbuildmat.2019.117924

Papadopoulos A, Hill C (2003) The sorption of water vapour by anhydride modified softwood. Wood Science and Technology 37(3):221–231. https://doi.org/https://doi.org/10.1007/s00226-003-0192-6

Perkowski Z, Świrska-Perkowska J, Gajda M (2017) Comparison of moisture diffusion coefficients for pine, oak and linden wood. Journal of building physics 41(2):135–161. https://doi.org/https://doi.org/10.1177/1744259116673967

Pittet V (1996) Etude expérimentale des couplages mécanosorptifs dans le bois soumis à variations hygrométriques contrôlées sous chargements de longue durée. Tech. rep., EPFL, https://doi.org/10.5075/epfl-thesis-1526

Ranta-Maunus A (1975) The viscoelasticity of wood at varying moisture content. Wood science and technology 9(3):189–205. https://doi.org/https://doi.org/10.1007/BF00364637

Ross RJ (2010) Wood Handbook: Wood as an Engineering Material. USDA Forest Service, Forest Products Laboratory

Silva C, Branco JM, Camões A, et al (2014) Dimensional variation of three softwood due to hygroscopic behavior. Construction and Building Materials 59:25–31. https://doi.org/https://doi.org/10.1016/j.conbuildmat.2014.02.037

Simpson WT (1993) Determination and use of moisture diffusion coefficient to characterize drying of northern red oak (quercus rubra). Wood Science and Technology 27(6):409–420. https://doi.org/https://doi.org/10.1007/BF00193863

Skaar C (1988) Electrical properties of wood. In: Wood-water relations. Springer, p 207–262, https://doi.org/https://doi.org$/10.1007/978-3-642-73683-4_6$

Sun X, He M, Li Z (2020) Novel engineered wood and bamboo composites for structural applications: State-of-art of manufacturing technology and mechanical performance evaluation. Construction and Building Materials 249:118,751. https://doi.org/https://doi.org/10.1016/j.conbuildmat.2020.118751

Thémelin A (1998) Comportement en sorption de produits ligno-cellulosiques. BOIS & FORETS DES TROPIQUES 256:55–67. https://doi.org/https://

doi.org/10.19182/bft1998.256.a19960

Tong D, Brown SA, Corr D, et al (2020) Wood creep data collection and unbiased parameter identification of compliance functions. Holzforschung 74(11):1011–1020. https://doi.org/https://doi.org/10.1515/hf-2019-0268

Tripathi J, Rice RW (2019) Finite element modelling of heat and moisture transfer through cross laminated timber panels. BioResources 14(3):6278–6293. https://doi.org/https://doi.org/10.1007/s10570-018-1898-9

Usta I (2005) A review of the configuration of bordered pits to stimulate the fluid flow. Maderas Ciencia y tecnología 7(2):121–132. https://doi.org/http://dx.doi.org/10.4067/S0718-221X2005000200006

Vishwakarma R, Shivhare U, Nanda S (2011) Moisture adsorption isotherms of guar (cyamposis tetragonoloba) grain and guar gum splits. LWT-Food Science and Technology 44(4):969–975. https://doi.org/https://doi.org/10.1016/j.lwt.2010.09.002

Weichert L (1963) Investigations on sorption and swelling of spruce, beech and compressed beech wood at temperatures between 20 c and 100 c. Holz Roh Werkst 21(8):290–300

Wood D, Vailati C, Menges A, et al (2018) Hygroscopically actuated wood elements for weather responsive and self-forming building parts–facilitating upscaling and complex shape changes. Construction and Building Materials 165:782–791. https://doi.org/https://doi.org/10.1016/j.conbuildmat.2017.12.134

Zelinka SL, Glass SV (2010) Water vapor sorption isotherms for southern pine treated with several waterborne preservatives. Journal of testing and evaluation Vol 38, no 4 (2010): p 1-5 Paper ID JTE102696 38(4):1–5. https://doi.org/https://doi.org/10.1520/jte102696

Zhang X, Zillig W, Künzel HM, et al (2015) Evaluation of moisture sorption models and modified mualem model for prediction of desorption isotherm for wood materials. Building and Environment 92:387–395. https://doi.org/https://doi.org/10.1016/j.buildenv.2015.05.021

Žlahtič-Zupanc M, Lesar B, Humar M (2018) Changes in moisture performance of wood after weathering. Construction and Building Materials 193:529–538. https://doi.org/https://doi.org/10.1016/j.conbuildmat.2018.10.196